Supporting Information

Table of Contents

S1. Electrolyte Compositions

The electrolyte compositions explored in this work are shown in **Tables S1-S2**. Note that the concentration is described according to the initial solution volume, not the final solution volume after dissolution, and is hence only an approximation of actual electrolyte concentration. The molality remains precisely defined before and after dissolution.

Table S1. Electrolyte compositions used in preliminary (anion and solvent effects) studies. EC/DMC refers to a mixture of EC and DMC in a 1:1 ratio, by weight.

Salt	Solvent	Salt Mass (g)	Solvent Mass (g)	Initial Molarity (mol L^{-1})	Molality (mol g^{-1})
$LiClO_4$	DMC	0.2171	2.0821	1.05	11.1
	EC/DMC	0.1064	1.0612	1.11	10.7
	PC	0.1073	1.2472	0.97	9.2
$LiBF_4$	DMC	0.1877	2.1355	1.00	8.2
	EC/DMC	0.0987	0.0983	1.25	94.1
	PC	0.0963	1.2375	1.00	7.3
$LiPF_6$	DMC	0.3049	2.0939	1.03	22.1
	EC/DMC	0.0924	0.6302	1.15	22.3
	PC	0.1525	1.2876	0.93	18.0
$LiSbF_6$	DMC	0.2435	1.0762	1.00	54.9
	EC/DMC	0.2434	1.1799	1.00	50.1
	PC	0.2830	1.2183	1.01	56.4
LiTFSI	DMC	0.2854	1.0251	0.96	79.9
	EC/DMC	0.2868	1.2245	0.96	67.2
	PC	0.2850	1.2073	1.02	67.8
LiFTFSI	DMC	0.2413	1.0975	0.99	52.1
	EC/DMC	0.2362	1.1691	1.00	47.9
	PC	0.2422	1.2430	0.99	46.2
LiFSI	DMC	0.1734	1.1313	0.88	28.7
	EC/DMC	0.1914	1.1906	1.01	30.1
	PC	0.1911	1.2073	1.02	29.6

Table S2. Electrolyte compositions used in optimization (concentration effects) studies. EC/DMC refers to a mixture of EC and DMC in a 1:1 ratio, by weight.

Salt	Solvent	Salt Mass (g)	Solvent Mass (g)	Initial Molarity (mol L^{-1})	Final Molarity (mol L^{-1})	Molality (mol kg^{-1})	OCV (V)
$LiPF_6$	EC/DMC	0.08	6.0	0.1	0.0982	0.08	2.65
	EC/DMC	0.76	6.0	1.0	0.9332	0.83	2.87
	EC/DMC	1.5	6.0	2.0	1.7881	1.7	3.13
	EC/DMC	2.3	6.0	3.0	2.5545	2.5	3.26
	EC/DMC	3.6	6.0	4.8	3.7904	4.0	3.39

S2. Open-Circuit Voltages

The open circuit voltage (OCV) for each cell composition is shown in **Table S3**.

Table S3. OCV as a function of cell configuration (in two-electrode cells containing Li metal as the counter electrode).

Salt	Solvent	Initial Molarity (mol L^{-1})	OCV (V)
$LiClO_4$	DMC	1.05	2.84
	EC/DMC	1.02	2.68
	PC	0.97	3.04
$LiBF_4$	DMC	1.00	3.23
	EC/DMC	1.05	3.40
	PC	1.00	3.10
$LiPF_6$	DMC	1.03	3.14
	EC/DMC	1.06	2.89
	PC	0.93	2.92
$LiSbF_6$	DMC	1.00	2.99
	EC/DMC	1.00	3.02
	PC	1.01	2.87
LiFSI	DMC	0.88	2.97
	EC/DMC	1.01	3.07
	PC	1.02	2.95
LiFTFSI	DMC	0.99	2.93
	EC/DMC	1.00	2.95
	PC	0.99	3.12
LiTFSI	DMC	0.96	2.79
	EC/DMC	0.96	3.09
	PC	1.02	3.05

S3. Electrochemical Screening Data (Voltage Opening)

The voltage opening experiments for all experiments carried out in the preliminary studies of all 21 final electrolytes are shown in **Figures S1a-S1c**.

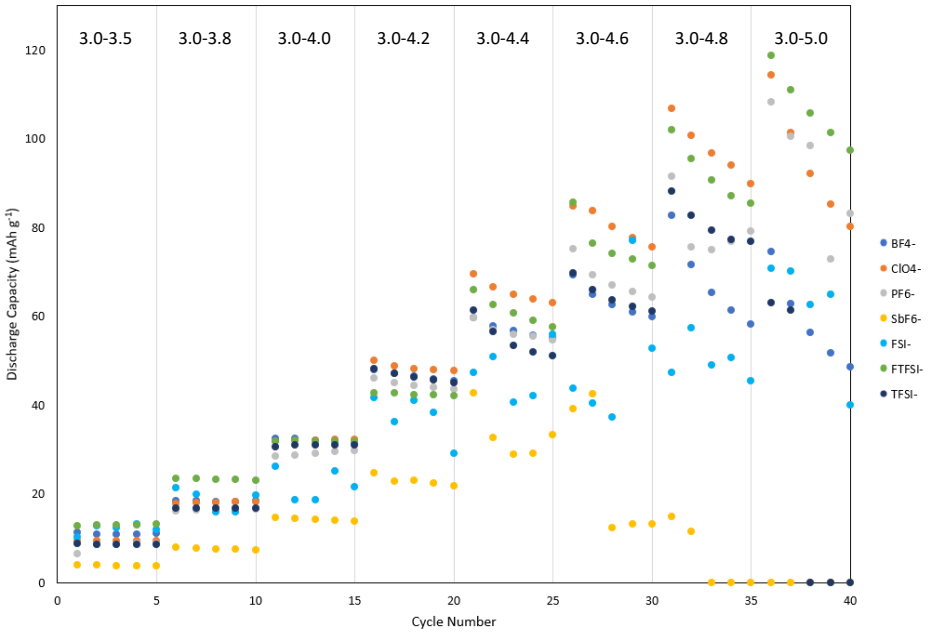

Figure S1a. Voltage opening dependencies (V vs. Li/Li^+) of 7 anions in EC/DMC at 100 mA g^{-1}.

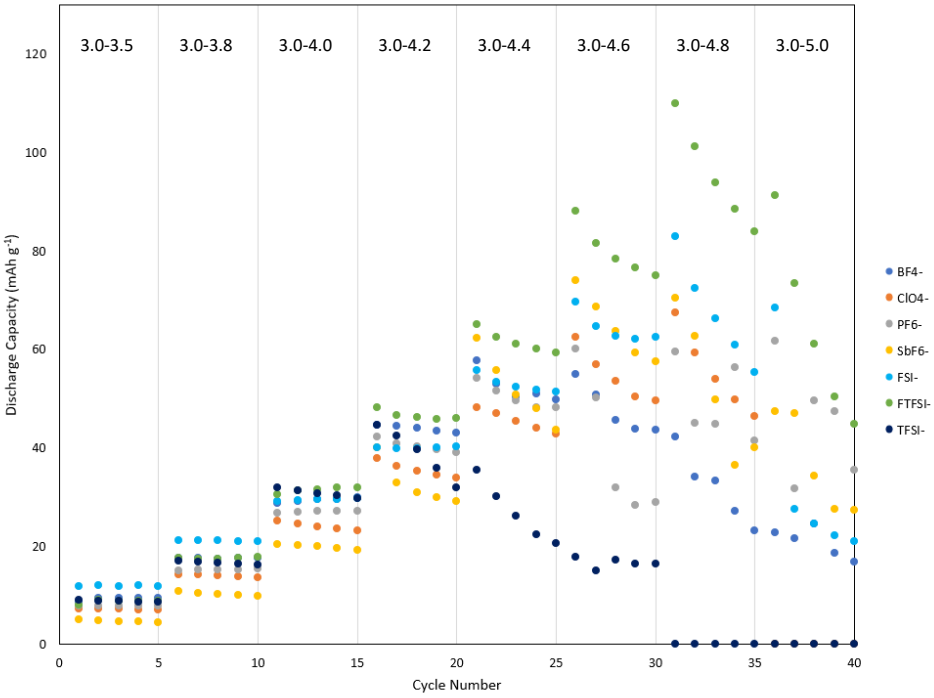

Figure S1b. Voltage opening dependencies (V vs. Li/Li^+) of 7 anions in DMC at 100 mA g^{-1}.

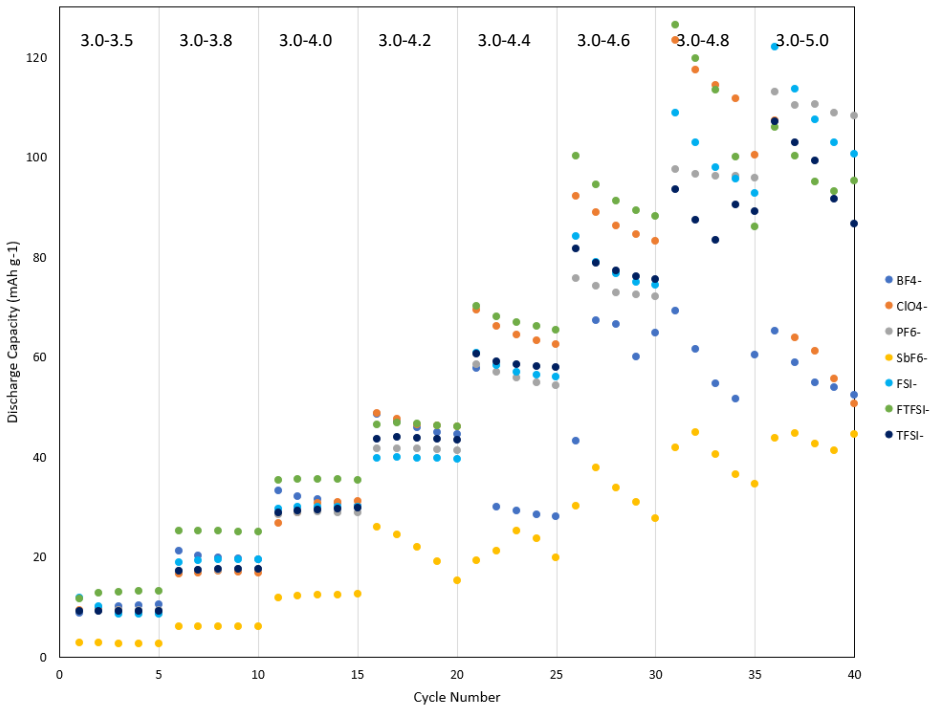

Figure S1c. Voltage opening dependencies (V vs. Li/Li^+) of 7 anions in PC at 100 mA g^{-1}.

S4. Electrochemical Screening Data (Current Rate)

The stepwise increasing current rate experiments carried out in the preliminary studies of all 21 final electrolytes are shown in **Figures S2a-S2c**.

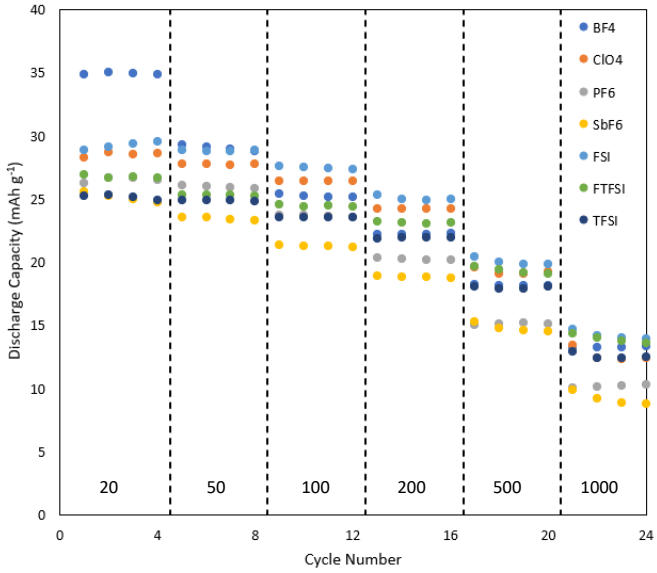

Figure S2a. Current rate dependencies (in mA g^{-1}) of 7 anions in PC cycled between 3.0-4.0 vs. Li/Li^+.

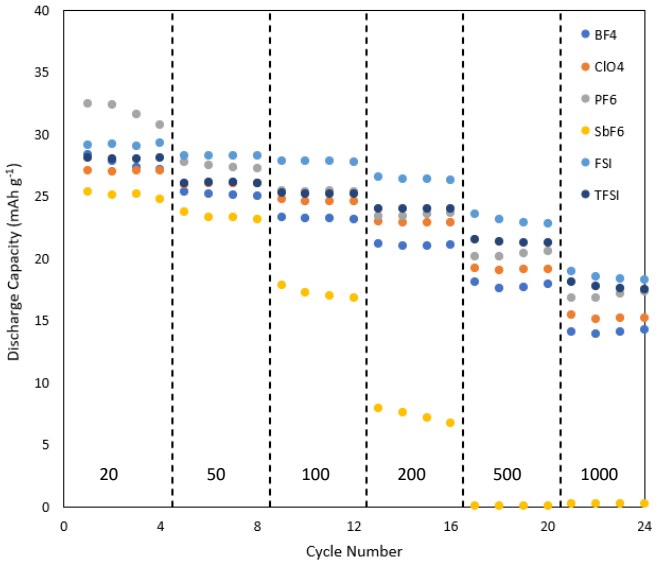

Figure S2b. Current rate dependencies (in mA g^{-1}) of 7 anions in EC/DMC cycled between 3.0-4.0 vs. Li/Li^+.

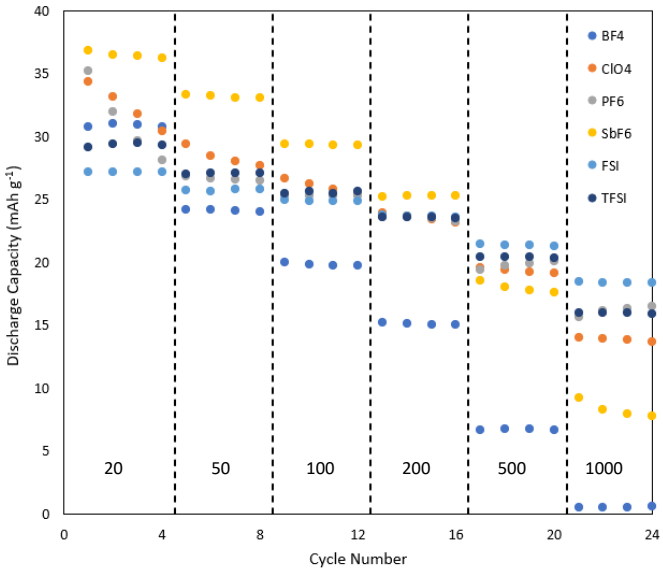

Figure S2c. Current rate dependencies (in mA g^{-1}) of 7 anions in DMC cycled between 3.0-4.0 vs. Li/Li^+.

S5. Solvent Properties

Viscosity and dielectric are closely correlated among the three solvents studied in this work, as shown in **Figure S3**. In general, solvent choice can affect ion-pairing, solvation thermodynamics, diffusion, decomposition stability, and co-insertion (solvation shell size, diffusivity, etc.).[13]

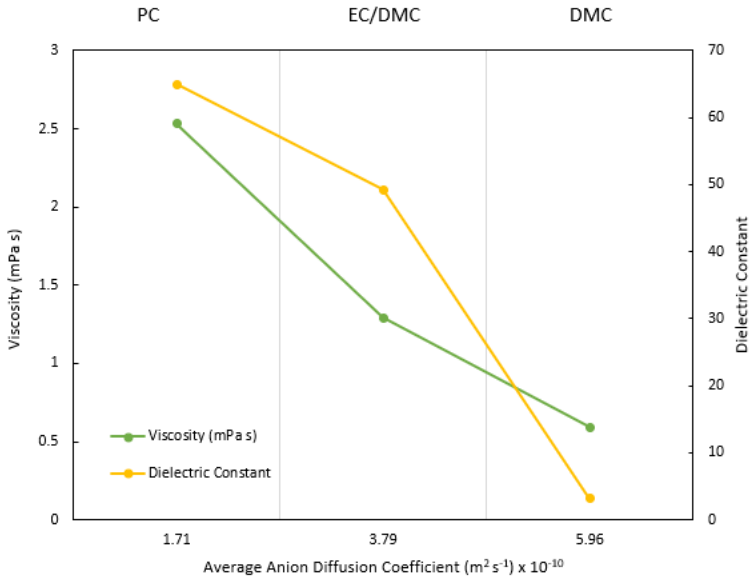

Figure S3. Viscosity and dielectric constant of PC, EC/DMC, and DMC as a function of the average anion diffusivity across all six fluorinated anions explored in this work.

Table S5. Solvent properties of PC, EC/DMC, and DMC.

	PC	**EC/DMC**	**DMC**
Viscosity (mPa s)	2.53	1.29	0.59
Dielectric Constant	64.96	49.21	3.12
Avg. Anion Diffusivity* (10^{-10} m^2 s^{-1})	1.71	3.79	5.96

*averaged over all fluorinated anions in this study

S6. Electrochemical Optimization Data ($LiPF_6$ in EC/DMC)

The voltage opening cycling voltammetry experiments carried out in the optimization studies of $LiPF_6$ in EC/DMC are shown in **Figure S4**. The lower potential cutoff of 2.5 V vs. Li/Li^+ was used to avoid undesirable Li^+ ion insertion in ZTC, as described in previous studies.[24]

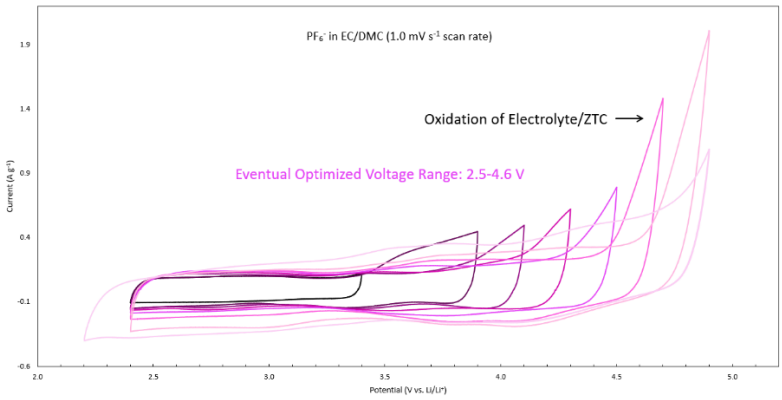

Figure S4. Cyclic voltammetry studies of 1.0 M $LiPF_6$ in EC/DMC at 1.0 mV s^{-1} cycled between 2.5-3.4 up to 2.5-4.9 V vs. Li/Li^+.

The voltage profiles for all experiments carried out in the subsequent optimization studies of $LiPF_6$ in EC/DMC are shown in **Figure S5**. The nominal concentrations are shown; actual concentrations are shown in **Table S2**.

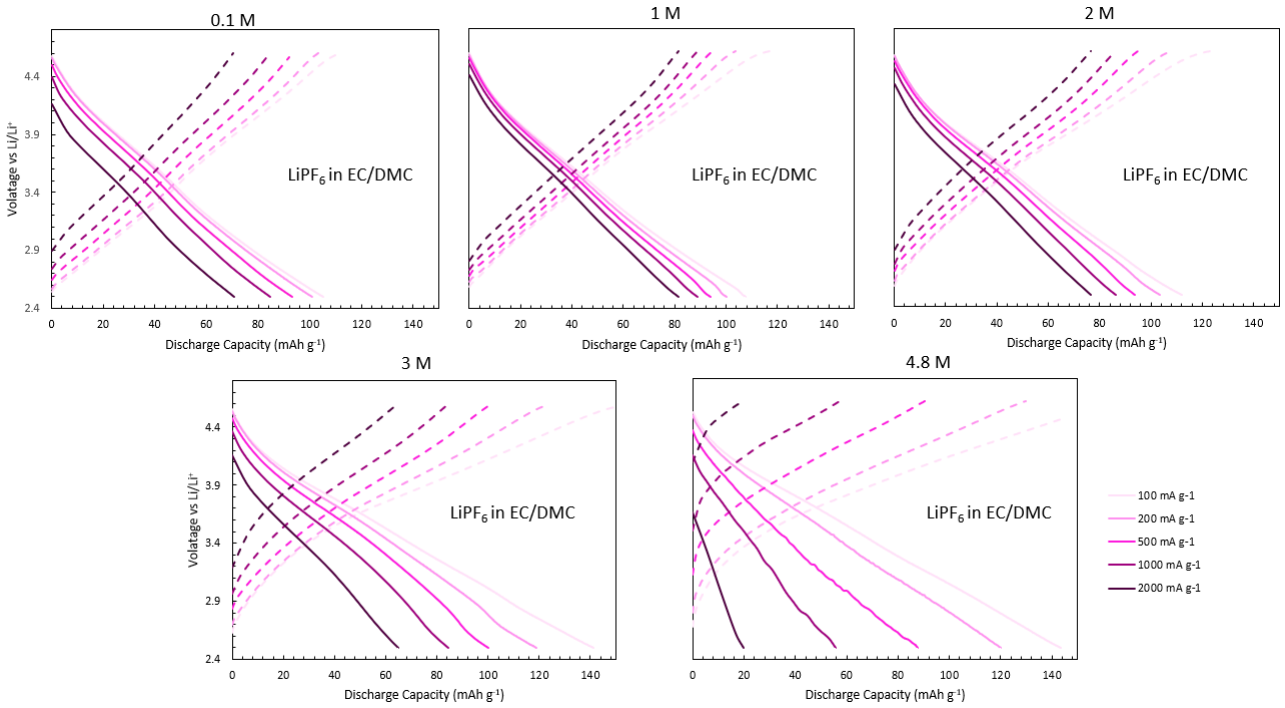

Figure S5. Voltage profiles for different concentrations of $LiPF_6$ in EC/DMC cycled between 2.5-4.6 V vs. Li/Li^+ and from 100 to 2000 mA g^{-1}.

Table S4. Anion, cation, and solvent diffusivity (in 10^{-10} m^2 s^{-1}) for $LiPF_6$ in EC/DMC at the five concentrations explored in this study.

Nominal Concentration (M)	Actual Concentration (M)	Li^+	PF_6^-	EC	DMC
0.1	0.0982	0.947	8.960	12.70	14.60
1.0	0.9332	0.414	4.170	5.27	6.32
2.0	1.7881	0.180	1.660	2.22	2.83
3.0	2.5545	0.047	0.396	0.50	0.56
4.8	3.7904	0.010	0.054	0.14	0.13

A Randles–Ševčík analysis of the insertion/deinsertion of PF_6^- within ZTC (1.0 M $LiPF_6$ in EC/DMC) is shown in **Figure S6**. Within the reduced 1.0 V window, charge storage in ZTC is purely capacitive with a B value of 0.94. In the wider 2.1 V window, more diffusive character is observed with a B value of 0.85.

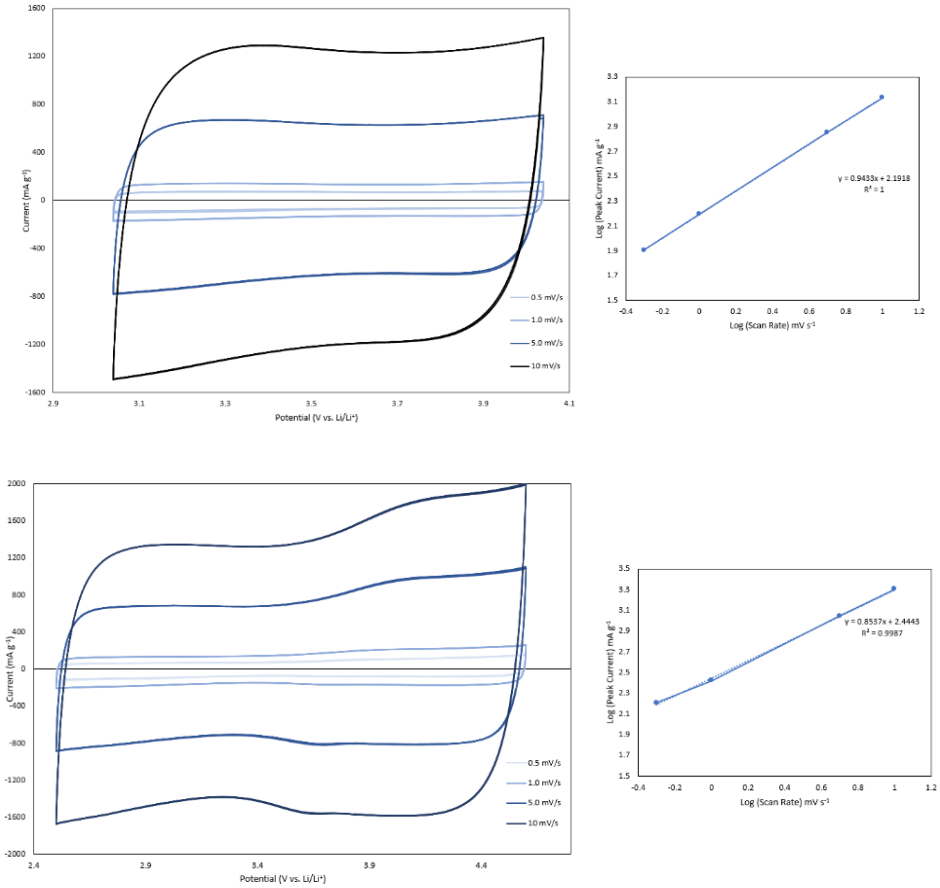

Figure S6. Cyclic voltammetry and Randles–Ševčík analysis between 3.0-4.0 V and 2.5-4.6 V vs. Li/Li^+ for 1.0 M $LiPF_6$ in EC/DMC. Separate cells were tested within each potential window and a total of three cycles were performed at each scan rate (0.5, 1.0, 5.0, and 10 mV s^{-1}).

S7. ZTC Synthesis and Characterization

ZTC was synthesized by a two-step (liquid/vapor) impregnation procedure. The zeolite NaY template (HSZ 320NAA, Tosoh Corp.) was degassed in a Büchi glass oven at 300 °C for 24 h under oil-free vacuum (<2 × 10^{-3} mbar). The dried zeolite (2 g) was then transferred (under Ar) into a 2-neck round bottom flask. The dried zeolite was combined with 20 mL of furfuryl alcohol (FA, 99% Aldrich) via syringe and the mixture was stirred at room temperature, under passive vacuum for 24 h. The impregnated solid was collected by vacuum filtration in air, washed three times with 10 mL aliquots of mesitylene (97%, Aldrich), and then dried under suction on the filter frit for 15 minutes. The impregnated and rinsed zeolite was placed in an alumina boat (10 × 30 × 107 mm) which was inserted into a quartz tube (ø 45 mm) installed in a horizontal tube furnace (HST 12/600, Carbolite Gero). The tube was purged under dry argon flow (200 sccm) at ambient pressure. The FA within the zeolite pores was first polymerized by heating up to 80 °C via a 10 min ramp and held for 24 h. The poly-FA was then carbonized by heating up to 700 °C via a 2 h ramp and held for 30 min. Further carbon impregnation was accomplished via propylene CVD at 700 °C for 5 h; the gas flow was switched to 7 mol% propylene in argon (99.99% propylene in 99.999% argon) at 200 sccm. An annealing step (under pure argon flow) was performed by heating the zeolite-carbon composite up to 900 °C via a 40 min ramp and held for an additional 1 h. The system was then cooled overnight, the gas flow was stopped, and the annealed zeolite-carbon composite was collected. Removal of the zeolite templated was accomplished by three sequential dissolutions in 35 mL of aqueous hydrofluoric acid (HF, 48-51%, ACROS Organics). The final ZTC product was collected by centrifugation, washed three times with 35 mL aliquots of distilled water, and then dried in air at 40 °C prior to electrode fabrication. Powder X-ray diffraction and N_2 adsorption/desorption isotherms of ZTC are shown in **Figure S7**.

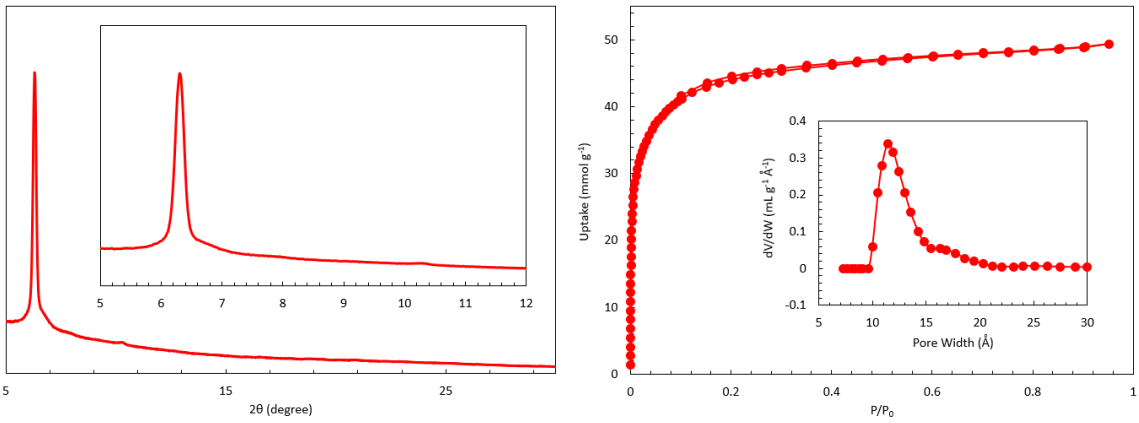

Figure S7. Materials characterization of ZTC: (left) X-ray diffraction pattern and (right) N_2 adsorption/desorption isotherm (77 K) and pore-size distribution.

S8. ZTC Supercage Calculations

Each ZTC unit cell (Nishihara Model II+[20] contains 64 supercages of the original zeolite template, where the void space of the original supercages becomes a "filled" region comprising the struts of the ZTC while the excluded volume of the original zeolite (its silicate framework) becomes the void space of the ZTC. Owing to the self-dual property of the diamond net (a simplification of the **FAU** structure), the number of supercages in faujasite is equal to the number of supercages in the corresponding **FAU**-ZTC. Thus, the conversion factor remains 64 supercages per unit cell. A single unit cell of Model II+ (a 2×2×2 supercell of the faujasite unit cell) has a lattice constant of a = 48.14 Å.

To determine the number of ions per supercage from the charge/discharge capacity in mAh g^{-1}, the equation below is used:

$$n = x\frac{\text{mAh}}{\text{g}} \times \frac{3.6\ \text{C}}{\text{mAh}} \times \frac{6.241 \times 10^{18}\ \text{e}^-}{\text{C}} \times \frac{1\ \text{anion}}{\text{e}^-} \times \frac{0.4626\ \text{g}}{\text{mL}} \times \frac{1.116 \times 10^{-19}\ \text{mL}}{\text{cell}} \times \frac{1\ \text{cell}}{64\ \text{supercages}}$$

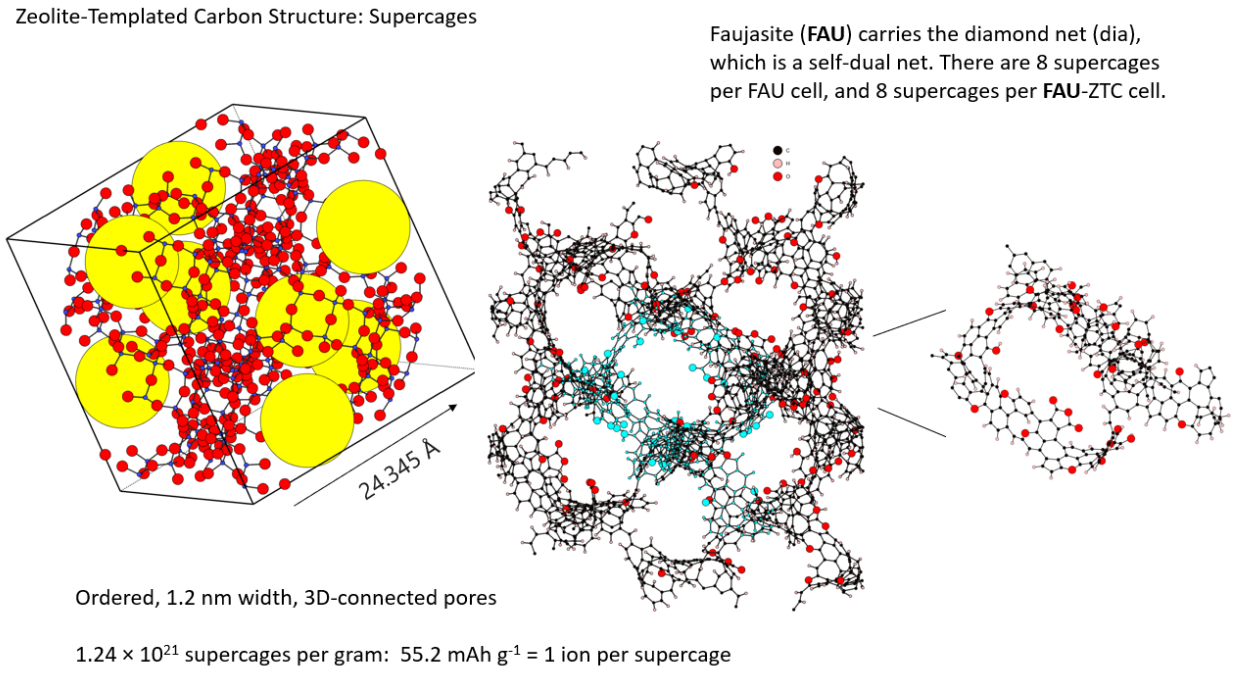

Figure S8. A representative ZTC "supercage".

S9. Binder Effects

Three different techniques were tested for the fabrication of ZTC electrodes: PVDF slurry cast on Cu foil, PTFE free-standing electrodes, and bare ZTC powder with no binder. The PVDF slurry did not adhere to the Cu foil and therefore could not be applied in electrochemical testing. The bare powder technique (no binder or additives) was chosen for all studies in this work due to its better performance over PTFE free-standing electrodes for capturing the "true" anion storage capacity of ZTC (**Figure S9**). The reduced capacity in PTFE electrodes can be attributed to pore-blocking.

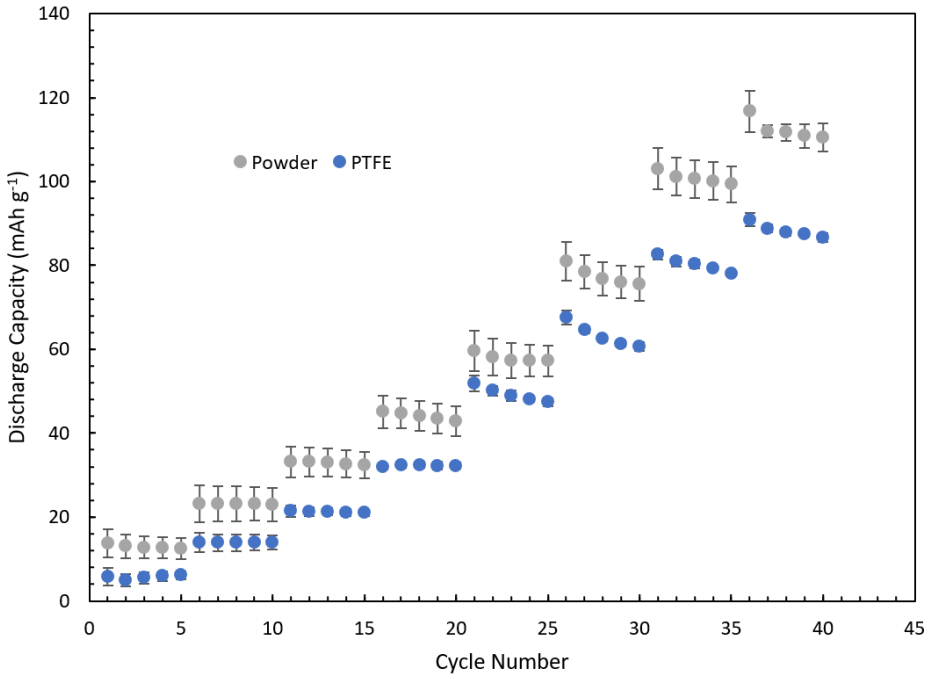

Figure S9. Direct comparison of ZTC electrodes formed by binding with PTFE and simply sprinkled into the cell without binder (as a bare powder). Error bars are standard deviations across all anions, tested in triplicate.

S10. Self-Discharge Analysis

Self-discharge was analyzed within a duplicate set of conditioned cells (i.e., after normal charge/discharge cycling at 100 mA g^{-1} for 9 complete cycles) comprising ZTC as the working electrode and 1.0 M $LiPF_6$ in EC/DMC as the electrolyte (**Figure S10**). After charging to 4.6 V vs. Li/Li^+ in the 10^{th} cycle, the cells were rested at open-circuit voltage (OCV) for 5 h, and then discharged to 2.5 V vs. Li/Li^+ as per the usual cycling protocol. A potential drop of 0.18 V was observed over the 5 h rest step, and a capacity loss of 8.7 mAh g^{-1} was observed upon cell discharge. This represents a 7% loss in capacity and may be attributable to anion leakage, or possibly to anion rearrangement leading to decreased anion deinsertion.

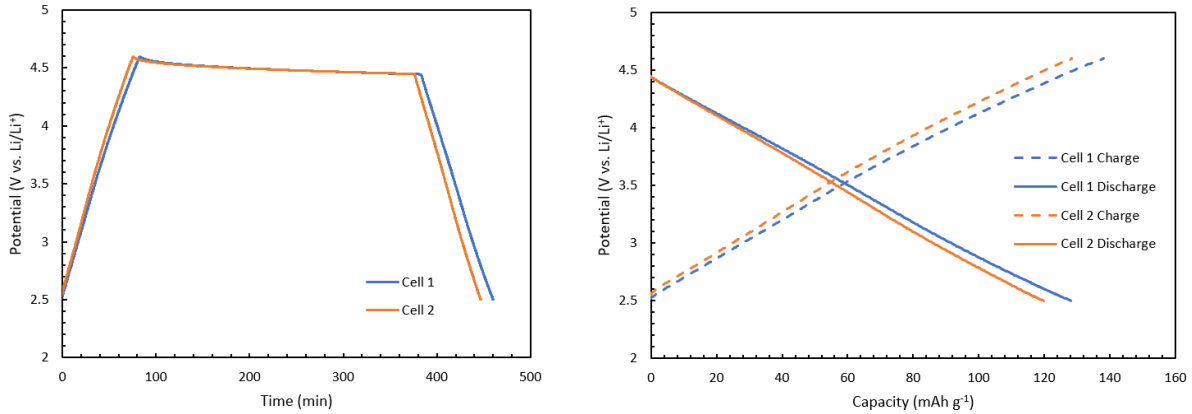

Figure S10. Self-discharge analysis of PF_6^- in ZTC, determined after 9 cycles of galvanostatic charge/discharge at 100 mA g^{-1} in the model electrolyte (1 M $LiPF_6$ in EC/DMC) at 2.5-4.6 V vs. Li/Li^+. (left) OCV as a function of time after the 10^{th} charge step, and (right) voltage profile comparison between the 10^{th} charge step and the 10^{th} discharge step, upon relaxation at OCV for 5 h in between.